Mathematical Biosciences and Engineering

MBE, 20 (3): 4760–4781.
DOI: 10.3934/mbe.2023220
Received: 25 November 2022
Revised: 20 December 2022
Accepted: 23 December 2022
Published: 30 December 2022

http://www.aimspress.com/journal/MBE

Research article

Dynamic analysis of the discrete fractional-order Rulkov neuron map

Gayathri Vivekanandhan[1], Hamid Reza Abdolmohammadi[2], Hayder Natiq[3], Karthikeyan Rajagopal[4], Sajad Jafari[5,6] and Hamidreza Namazi[7,8,*]

[1] Department of Computerscience Engineering, Chennai Institute of Technology, Chennai 600069, Tamil Nadu, India
[2] Electrical and Computer Engineering Group, Golpayegan College of Engineering, Isfahan University of Technology, Golpayegan, 87717-67498, Iran
[3] Department of Computer Technology Engineering, College of Information Technology, Imam Ja'afar Al-Sadiq University, Baghdad, Iraq
[4] Centre for Nonlinear Systems, Chennai Institute of Technology, Chennai 600069, Tamil Nadu, India
[5] Department of Biomedical Engineering, Amirkabir University of Technology (Tehran polytechnic), Iran
[6] Health Technology Research Institute, Amirkabir University of Technology (Tehran polytechnic), Iran
[7] College of Engineering and Science, Victoria University, Melbourne, Australia
[8] School of Engineering, Monash University, Selangor, Malaysia

*** Correspondence:** Email: Hamidreza.namazi@monash.edu.

Abstract: Human evolution is carried out by two genetic systems based on DNA and another based on the transmission of information through the functions of the nervous system. In computational neuroscience, mathematical neural models are used to describe the biological function of the brain. Discrete-time neural models have received particular attention due to their simple analysis and low computational costs. From the concept of neuroscience, discrete fractional order neuron models incorporate the memory in a dynamic model. This paper introduces the fractional order discrete Rulkov neuron map. The presented model is analyzed dynamically and also in terms of synchronization ability. First, the Rulkov neuron map is examined in terms of phase plane, bifurcation diagram, and Lyapunov exponent. The biological behaviors of the Rulkov neuron map, such as silence, bursting, and chaotic firing, also exist in its discrete fractional-order version. The bifurcation diagrams of the proposed model are investigated under the effect of the neuron model's parameters and the fractional order. The stability regions of the system are theoretically and numerically obtained, and it is shown that increasing the order of the fractional order decreases the stable areas. Finally, the synchronization behavior of two fractional-order models is investigated. The results represent that the fractional-order systems cannot reach complete synchronization.

Keywords: discrete fractional-order; Rulkov neuron map; stability analysis; bifurcation; synchronization

1. Introduction

Computational neuroscience studies the function of the brain from different molecular, cellular and behavioral levels [1]. The mathematical neuronal models are used to evaluate the qualitative function of neurons [2,3]. A wide variety of neural activities, such as different firing patterns, can be represented by neuronal models [4–8]. Neuronal models are generally divided into continuous time and discrete time. Continuous time neuronal models are described by the ordinary differential equations (ODE) such as Hodgkin-Huxley [9], Fitzhugh-Nagumo [10,11], and Hindmarsh-Rose [12,13]. For example, Njitack and colleagues examined the effect of a memristive autapse on the dynamics of a two-dimensional Hindmarsh–Rose neuron [14]. In another work, the effect of a two-dimensional FitzHugh–Nagumo, along with a 3D Hindmarsh–Rose neuronal model, was evaluated by coupling a multistability memristive synapse [15]. Models of continuous time neurons have been extensively studied dynamically, while less attention has been paid to the map-based discrete time models [16]. The distinctive features of discrete-time neuron maps are their high potential for complex behavior modeling, memory savings, and simplifying large neural network calculations [17,18]. Therefore, many scientists have tried to introduce discrete-time neuron maps [19]. For example, with the Euler discretization of the Hodgkin-Huxley neuronal model, the Izhikevich neuronal model was introduced [20]. The Nagumo-Sato discrete neuronal model was proposed in 1972 [21], and in 1990 a modified version of this model was introduced[22]. A one-dimensional map-based neuronal model of self-interaction was proposed in 1997 by Pasemann [23]. In 2001, Rulkov proposed a simple two-dimensional turbulent neuron model, one of the first phenomenological models to show a variety of basic neural behaviors (bursts of spikes, spikes, silence) [24]. Mathematical modeling of bursts and some spikes is impossible in the context of two-dimensional continuous-time systems, but Rulkov's two-dimensional model can demonstrate these behaviors [25].

The dynamic behaviors of the coupled Rulkov neuron map have been studied in recent research [26–28]. Sun et al. investigated the complete synchronization of Rulkov chaotic neural networks using master stability function analysis [29]. Franović investigated the effects of synaptic time delay on Rulkov map neurons with chemical coupling [30]. Rakshit et al. examined the stabilization, neural synchronization, and dynamics of two coupled Rulkov neurons with electrical and chemical synaptic interactions [31]. Wagemakers et al. introduced an electronic implementation of the Rulkov neuron map [32]. Li et al. proposed a discrete memristive neuron model based on the Rulkov model, which can better describe the actual firing activity of biological neurons due to biophysical memory [33]. Cheng et al. studied the synchronization dynamics of two heterogeneous chaotic Rulkov neurons with electrical synapses [34]. It is notable that the target for synchronization stability means energy balance between neurons and the neurons reach energy balance after complete synchronization [35,36].

Discrete fractional calculus has been used in the dynamic analysis of map-based systems. The fractional-order derivatives are relatively more accurate than actual order derivatives because they are an effective tool for describing the effect of memory on processing [37]. Memory effects in fractional order indicate that all previous models are involved in determining the system modes [38]. Over the

past several years, researchers have focused on incorporating the fractions in various applications of neural networks, physics, biology, etc. [39–43]. The discrete fraction order equation is also a powerful tool in modeling chaotic systems [44–46]. For example, Guo-Cheng et al. reported the delayed logistic equation using the discrete fractional calculus approach and the corresponding discrete perturbation [47]. Elsonbaty et al. proposed a susceptible-infected-treatment-recovered-susceptible (SITRS) fractional discrete model to simulate the coronavirus (COVID-19) epidemic [48]. Kassim et al. developed a secure image transfer scheme based on synchronizing turbulent time-discrete fractional systems [49]. Fractional derivative properties can be expressed in the biological sense as follows [50]:

1. The fractional-order derivative represents the inheritance characteristics more accurately compared to integer-order models.
2. FO neuron models correctly represent biological properties in the presence of noise, which full-order models fail to do.
3. Dynamic firing activities of multiple time scales for a single neuron can be treated with FO derivatives.
4. Firing frequency responses are better in fractional designs than in integer models.
5. Dynamic excitatory properties reveal several neurocomputational properties that can be achieved in FO systems, which enrich functional neural mechanisms.

In general, human evolution is done by two genetic systems based on DNA and another based on the transmission of information through the functions of the nervous system. Mechanisms underlying neuron-based inheritance include hippocampal neurogenesis and memory and learning processes that generate new neural complexes and alter brain structure and function [51]. From the concept of neuroscience, the discrete fractional order models the neuron's hereditary behaviors as memory in the dynamic model. Given the above, this paper aims to assist researchers in computational neuroscience by introducing a discrete fraction order derivative to the Rulkov neuronal model. The dynamics of the fractional order map is analyzed completely and, in the end, its synchronization is examined. Synchronization of neurons has become an interesting topic in recent years [26,52,53] due to its critical applications in the neural processes [54,55]. This paper includes the following sections: Section 2 introduces the Rulkov neuron map, demonstrating the system's dynamic and biological behaviors. Section 3 presents a discrete fractional order Rulkov neuron map and dynamically evaluates the effect of fractional order and model parameters. In section 4, the fixed points are calculated, and their stability is examined. Section 5 investigates the synchronization of two fractional-order Rulkov neurons in different fractional orders, and finally, Section 6 gives conclusions.

2. Mathematical Rulkov neuron map

In this section, Rulkov neuron map is introduced as a discrete system. Rulkov neuron map is a discrete biological neuronal model proposed by Nikolai F. Rulkov in 2001 [24,25]. This model, in which n indicates the discrete time, is defined as follows:

$$x_{n+1} = \frac{\alpha}{1+x_n^2} + y_n, \tag{2.1}$$

$$y_{n+1} = y_n - \mu(x_n - \sigma), \tag{2.2}$$

where the variable x_n is the membrane potential of neurons, and the variable y_n in the model is a

system-slowing variable due to the minimal value of μ ($0 < \mu << 1$). Unlike the variable x_n, the variable y_n has no clear biological meaning [30]. The parameter σ is an external dc current to neurons, and the parameter α is a nonlinear map parameter. The value of μ is always considered 0.001. By changing the parameters σ and α of the system, different behaviors such as silence ($\sigma = -2, \alpha = 6.22$), bursting ($\sigma = -1, \alpha = 4.1$) and chaotic firing ($\sigma = -1, \alpha = 5.7$) can be seen which are shown in Figure 1 for random initial conditions. Phase diagram for burst mode and chaotic firing mode are shown in parts (d) and (e) of Figure 1.

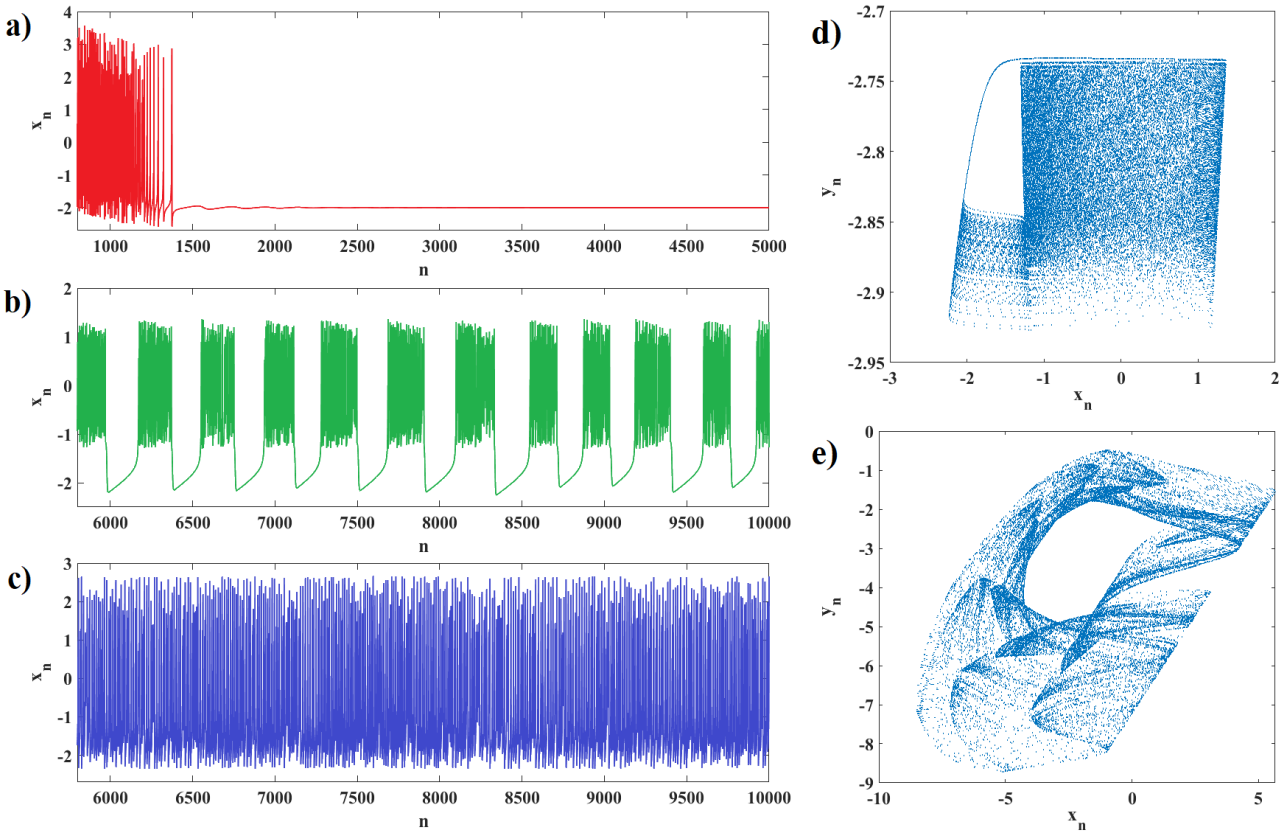

Figure 1. By changing the parameters σ and α, different behaviors of the system such as **(a)** silence ($\sigma = -2, \alpha = 6.22$), **(b)** bursting ($\sigma = -1, \alpha = 4.1$), and **(c)** chaotic firing ($\sigma = -1, \alpha = 5.7$) are observed with random initial condition. Phase diagram of **(d)** bursting and **(e)** chaotic firing for Rulkov neuron map using the random initial conditions between -1 and 1.

In continuation, the dynamic analysis of the Rulkov neuron map is performed through bifurcation diagrams and the maximum Lyapunov exponents (MLE) calculations. The positive MLE proves the existence of chaotic behavior. The bifurcation diagram is plotted by changing the parameter α in the range of 4 to 20 with random initial conditions in the range of $[-1, 1]$ for the variable x_n in part (a) and for the variable y_n in part (b) of Figure 2. Also, the MLE of the model for parameter α is shown in part (c) of Figure 2 ($\sigma = -0.1, \mu = 0.001$). It can be seen that with the change of α in the interval $[4, 4.725]$, the neuron's firing is period one (MLE is zero) and then enters chaos in $\alpha = 4.725$ until $\alpha = 8.576$. At $\alpha = 8.576$, the firing changes to periodic and again by period doubling enters another chaotic region in $\alpha = 14.688$, and finally exits from chaos in $\alpha = 19.280$. There is also a periodic

window in the interval $[16.213, 16.327]$. The bifurcation diagram for variables x_n and y_n with respect to variation of parameter σ in the range of $[-2.5, 0]$ are shown in parts (d) and (e) of Figure 2 ($\alpha = 4.1$, and $\mu = 0.001$). The corresponding MLE is drawn in part (f) of Figure 2. By changing σ, the dynamic behavior is periodic for the interval $[-2.5, -1.632]$, $[-1.632, -0.145]$, and then switches to chaotic. The bifurcation diagrams by changing parameter μ in the interval $[0, 1]$ for $\alpha = 4.1$, and $\sigma = -0.1$ are shown in parts (g) and (h) of Figure 2 for variables x_n and y_n. By changing the μ parameter, the chaotic behavior is seen in the intervals $[0, 0.087]$ and $[0.377, 0.805]$.

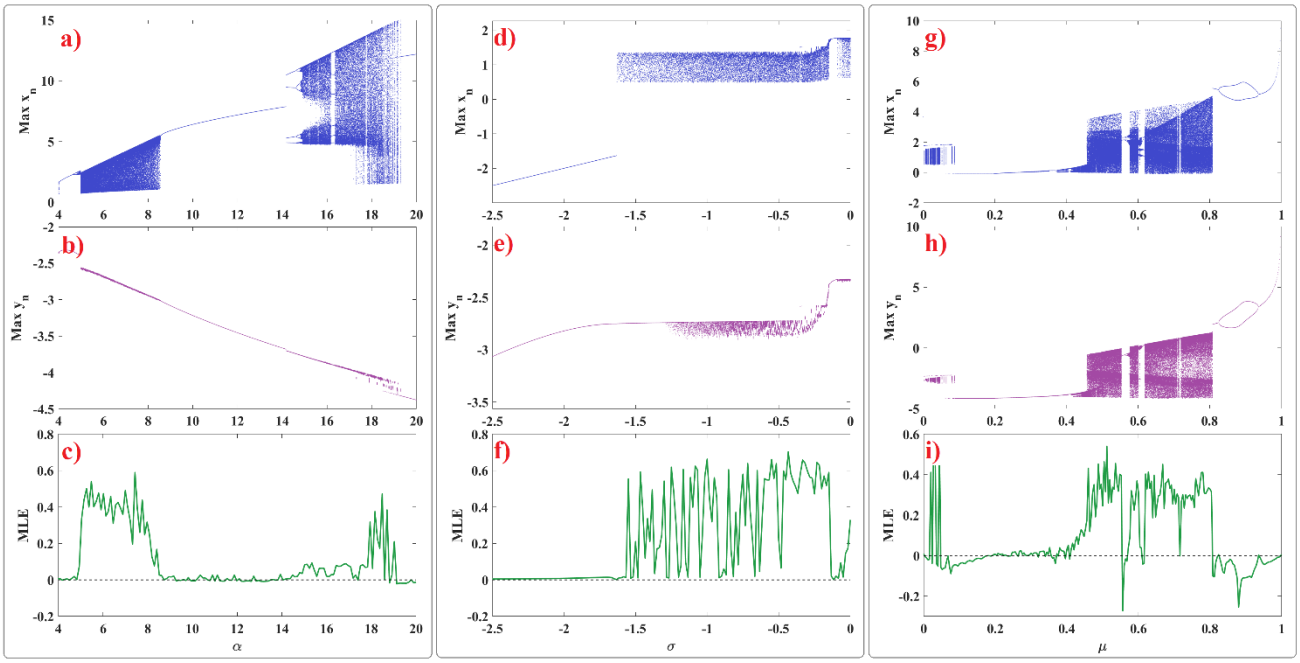

Figure 2. Left panel: The bifurcation diagram by changing the parameter α in the range $[4, 20]$ for **(a)** the variable x_n, and **(b)** the variable y_n, and its corresponding maximum Lyapunov exponent (MLE) diagram **(c)** in $\sigma = -0.1$, $\mu = 0.001$. Middle panel: The bifurcation diagram by changing the parameter σ in the range $[-2.5, 0]$ for **(d)** the variable x_n, and **(e)** the variable y_n, and its corresponding maximum Lyapunov exponent (MLE) diagram **(f)** in $\alpha = 4.1$, $\mu = 0.001$. Right panel: The bifurcation diagram by changing the parameter μ in the range $[0, 1]$ for **(g)** the variable x_n, and **(h)** the variable y_n, and its corresponding maximum Lyapunov exponent (MLE) diagram **(i)** in $\alpha = 4.1$, $\sigma = -0.1$.

3. Fractional-order discrete Rulkov neuron map

In this section, Rulkov neuron map is reformulated as a fractional-order discrete system using the Caputo left difference operator. Discrete fraction order maps have recently been recognized as a new powerful tool in modeling and describing the dynamics of complex nonlinear discrete systems [56,57]. Different numerical methods have been developed to solve discrete fraction order maps [58,59]. In this paper, we examine the following Rulkov neuron map with discrete fraction order:

$$\Delta_a^q x(t) = \frac{\alpha}{1+x(t+q-1)^2} + y(t+q-1), \tag{3.1}$$

$$\Delta_a^q y(t) = y(t+q-1) - \mu(x(t+q-1) - \sigma), \tag{3.2}$$

$$t \in N_{a+1-q},\ x(0) = c_1, y(0) = c_2\ , 0 < q,$$

where Δ_a^q is a function of the Caputo delta difference on the left, $N_a = [a, a+1, a+2, \dots]$ represents the time scale isolated ($a \in R$ and constant). To obtain the fractional order form of the Rulkov neuron map, we first define the necessary definitions from the discrete fractional calculus and generalize the results to the Rulkov neuron map.

Definition 1. When $u: N_a \to R$, $q > 0$ and $q \notin N$, the sum of the fraction of order q is defined as follows:

$$\Delta_a^{-q} u(t) \coloneqq \frac{1}{\Gamma(q)} \sum_{s=a}^{t-q} \quad (t-s-1)^{(q-1)} u(s), t \in N_{a+q}, \tag{3.3}$$

where a is the starting point, and $t^{(q)}$ is the falling function, which is defined as follows:

$$t^{(q)} = \frac{\Gamma(t+1)}{\Gamma(t-q+1)} = t(t-1) \dots (t-q+1), \tag{3.4}$$

where $\Gamma(t)$ is Gamma function, defined as follows [60]:

$$\Gamma(t) = \int_0^{\infty} \quad x^{q-1} e^{-x} dx \tag{3.5}$$

Definition 2. For $q > 0$, $q \in N_a$ and $u(t)$ defined on N_a, the difference in the Caputo delta fraction can be expressed as follows [58]:

$$\Delta_a^q u(t) := \Delta_a^{-(m-q)} \Delta^m u(t) = \frac{1}{\Gamma(m-q)} \sum_{s=a}^{t-(m-q)} \quad (t-s-1)^{(m-q-1)} \Delta^m u(s), \tag{3.6}$$

where $m = [q] + 1$ and $m = [q] + 1$.

Theorem 1. *For the delta fraction difference equation*

$$\Delta_a^q u(t) = f\big(t+q-1, u(t+q-1)\big), \quad \Delta^k u(a) = u_k, \quad m = [q]+1, k = 0, \dots, m-1, \tag{3.7}$$

the equivalent discrete integral equation can be obtained as follows:

$$u(t) = u_0(t) + \frac{1}{\Gamma(q)} \sum_{s=a+m-q}^{t-q} \quad (t-s-1)^{(q-1)} f\big(s+q-1, u(s+q-1)\big),\ t \in N_{a+m}, \tag{3.8}$$

where the initial iteration $u_0(t)$ is expressed as follows:

$$u_0(t) = \sum_{k=0}^{m-1} \quad \frac{(t-a)^{(k)}}{k!} \Delta^k u(a). \tag{3.9}$$

Detailed descriptions of the above results are given in reference [61].

Rulkov's neural map of discrete fraction order (Eq. 3.1, and Eq. 3.2) can be written as the following classical map:

$$\Delta x(n) = \frac{\alpha}{1+x(n)^2} + y(n), \qquad x(0) = c_1, \tag{3.10}$$

$$\Delta y(n) = y(n) - \mu(x(n) - \sigma), \qquad y(0) = c_2. \tag{3.11}$$

According to Theorem 1, we can write the discrete fractional for Rulkov's model in the following

form:

$$x(t) = x(0) + \frac{1}{\Gamma(q)}\sum_{s=1-q}^{t-q} \quad (t-s-1)^{(q-1)}\left(\frac{\alpha}{1+\left(x(s+q-1)\right)^2} + y\big(x(s+q-1)\big)\right), \tag{3.12}$$

$$y(t) = y(0) + \frac{1}{\Gamma(q)}\sum_{s=1-q}^{t-q} \quad (t-s-1)^{(q-1)}\big(y(s+q-1) - \mu(x(s+q-1)-\sigma)\big). \tag{3.13}$$

In conclusion, the numerical formula of the n-dependent discrete Rulkov fractional neuronal model is defined as follows:

$$x(n) = x(0) + \frac{1}{\Gamma(q)}\sum_{i=1}^{n} \quad \frac{\Gamma(n-i+q)}{\Gamma(n-i+1)}\left(\frac{\alpha}{1+x_{i-1}^2} + y_{i-1}\right), \tag{3.14}$$

$$y(n) = y(0) + \frac{1}{\Gamma(q)}\sum_{i=1}^{n} \quad \frac{\Gamma(n-i+q)}{\Gamma(n-i+1)}\big(y_{i-1} - \mu(x_{i-1}-\sigma)\big). \tag{3.15}$$

The difference between the maps of the integers of Eq. 2.1, and Eq. 2.2 and the fractional order of Eq. 3.14, and Eq. 3.15 is a discrete core function and $x(n)$ and $y(n)$ refer to the past information $x(0), \dots, x(n-1)$ and $y(0), \dots, y(n-1)$. As a result, the current state depends on all past forms, which express the memory effects. We define the proposed model in Eq. 3.14, and Eq. 3.15 as the fractional-order of discrete Rulkov neuron map (FORNM). Also, in Eq. 3.14, and Eq. 3.15, the following equation is used:

$$\frac{\Gamma(n-i+q)}{\Gamma(n-i+1)} = e^{lnln\,\Gamma(n-i+q)-\Gamma(n-i+1)}. \tag{3.16}$$

By changing the parameters α, σ, and μ of the FORNM system, different behaviors such as silence ($\alpha = 3.15$, $\sigma = -2$, $\mu = 0.2$, $q = 0.001$), bursts of spikes ($\alpha = 3.5$, $\sigma = -2$, $\mu = 0.2$, $q = 0.001$), and chaotic firing ($\alpha = 6$, $\sigma = -1$, $\mu = 0.3$, $q = 0.001$) can be seen which are shown in Figure 3. When the membrane potential reaches a threshold, the neuron fires and generates a signal that travels to other neurons, which in turn increases or decreases their potential in response to the signal. The neuron model that fires when the threshold is crossed is called a spiking neuron. Neuron spiking occurs when up-down oscillations accompany this spike train [62,63]. According to the stated definition, bursts of spikes occurs in part (b) of Figure 3, and this spiking behavior has been previously identical in [24,31]. The phase diagram for the bursts of spikes mode is shown in part (d) and for the chaotic firing in part I.

In the following, the dynamical analysis of the FORNM is done by plotting the bifurcation diagrams versus the fractional order (q) and the system parameters at different intervals.

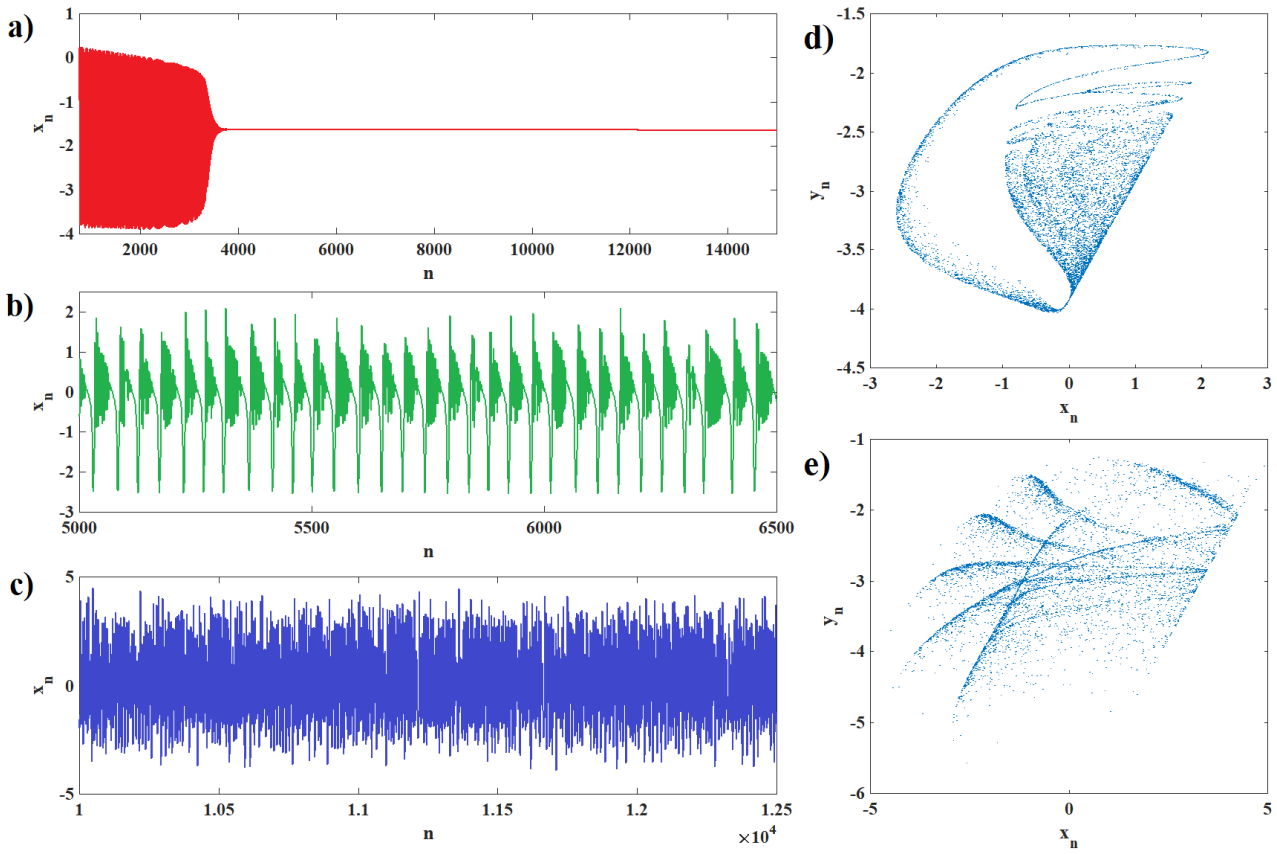

Figure 3. Time series of **(a)** silence ($\alpha = 3.1, \sigma = -2, \mu = 0.2, q = 0.001$) with initial condition $[0.1, 0.1]$, **(b)** bursts of spikes ($\alpha = 3.5, \sigma = -2, \mu = 0.2, q = 0.001$) with initial condition $[0.4, 0.4]$ and **(c)** chaotic firing ($\alpha = 6, \sigma = -1, \mu = 0.3, q = 0.001$) with initial condition $[0.2, 0.2]$, along with the phase diagram for the **(d)** bursts of spikes and I chaotic firing mode are shown.

3.1. Effect of the FORNM parameters

The dynamic behavior of the FORNM is firstly investigated by changing the parameters of the Rulkov neuron map. It was shown that there are chaotic, periodic, and fixed-point dynamics in the system for different values of parameters α, σ, and μ. Figure 4 shows the bifurcation diagrams wherein the left, middle, and right columns, the fractional order is set to $q = 0.001$, $q = 0.01$, and $q = 0.02$, respectively. The bifurcation parameter in parts (a-c) is α in the interval $[0, 12]$ for $\sigma = -1$ and $\mu = 0.3$, and in parts (d-f) is σ in the interval $[-5, 0]$ for $\alpha = 4$ and $\mu = 0.3$, and in parts (g-i) is μ in the Interval $[0.15, 0.5]$ for $\alpha = 4$ and $\sigma = -1$. The initial conditions are selected randomly. It can be observed that the dynamics are strongly dependent on q. Generally, it can be concluded that by increasing q, the chaotic behavior is observed for higher bifurcation parameters, and the region of chaotic behavior is shrunken.

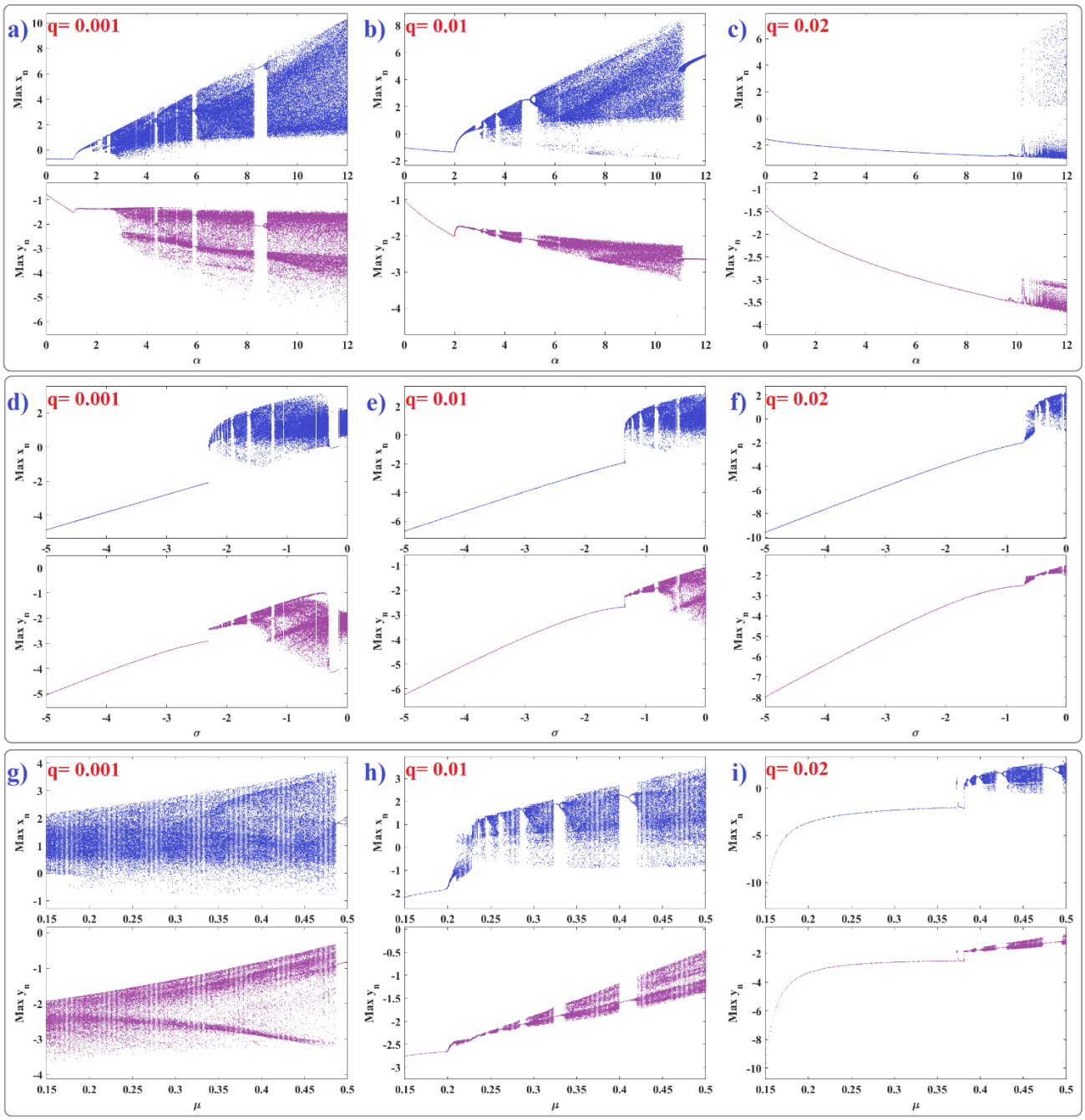

Figure 4. The bifurcation diagrams by changing the model parameters for the variables x_n and y_n. Upper panel: by varying α in the interval $[0, 12]$ for **(a)** $q = 0.001$, **(b)** $q = 0.01$, and **(c)** $q = 0.02$ ($\sigma = -1$, $\mu = 0.3$). Middle panel: by varying σ in the interval $[-5, 0]$ for **(d)** $q = 0.001$, **(e)** $q = 0.01$, and **(f)** $q = 0.02$ ($\alpha = 4$, $\mu = 0.3$). Lower panel: by varying μ in the interval $[0.15, 0.5]$ for **(g)** $q = 0.001$, **(h)** $q = 0.01$, and **(i)** $q = 0.02$ ($\alpha = 4$, $\sigma = -1$). The initial conditions are random.

3.2. Effect of the fractional-order

Another important factor in FORNM is the fractional order parameter, which can affect the overall dynamics. Figure 5 presents the bifurcation diagrams of the model according to the fractional order for

different parameter values. The bifurcation diagram for $\alpha = 1.9$, $\sigma = -1$, $\mu = 0.3$ in part (a) of Figure 5 shows chaotic behavior for the range $[0, 0.0102]$ and periodic behavior for the range $[0.0102, 0.1]$. In part (b), in which $\alpha = 4.9$, $\sigma = -1$, $\mu = 0.3$ the chaos is seen in the range of $[0, 0.0180]$. The bifurcation diagram in terms of q for $\sigma = -2$, $\alpha = 4$, and $\mu = 0.3$ is shown in part (c) that has chaotic behavior for the interval $[0, 0.00389]$, while for $\sigma = -0.833$ in part (d), the chaotic behavior happens in $[0, 0.01928]$. The bifurcation diagram for $\mu = 0.33$, $\alpha = 4$, and $\sigma = -1$ is shown in part (e) of Figure 5. In this case, the chaotic behavior is in the range $[0, 0.01809]$. In part (f) where $\mu = 0.45$, two chaotic regions in $[0, 0.2928]$ and $[0.1860, 0.2]$ are observed. As shown in Figure 5, increasing the parameters' values increases the chaotic region.

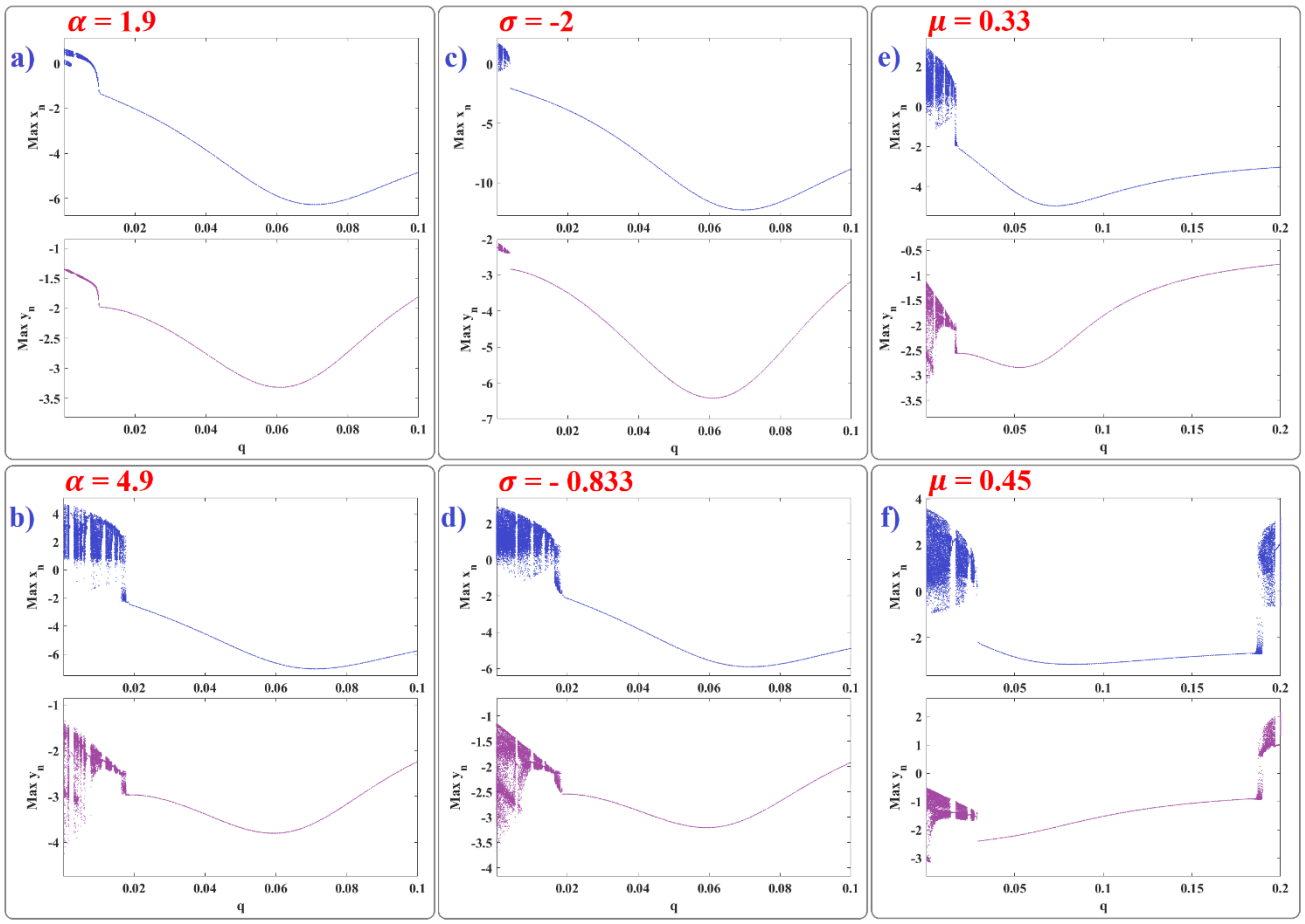

Figure 5. The bifurcation diagrams by changing the parameter q for the variable x_n and y_n with random initial conditions. **(a)** $\alpha = 1.9$, $\sigma = -1$, $\mu = 0.3$, **(b)** $\alpha = 4.9$, $\sigma = -1$, $\mu = 0.3$, **(c)** $\alpha = 4$, $\sigma = -2$, $\mu = 0.3$, **(d)** $\alpha = 4$, $\sigma = -0.833$, $\mu = 0.3$, **(e)** $\alpha = 4$, $\sigma = -1$, $\mu = 0.33$, and **(f)** $\alpha = 4$, $\sigma = -1$, $\mu = 0.45$.

4. Fixed points and stability analysis of FORNM

In this section, we calculate the equilibrium points of the proposed FORNM of Eq. 3.14, and Eq. 3.15 and evaluate them in terms of stability. The equilibrium points are calculated by:

$$\frac{\alpha}{1+x(n)^2} + y(n) = 0, \tag{4.1}$$

$$y(n) - \mu(x(n) - \sigma) = 0, \tag{4.2}$$

i.e.

$$y(n) = -\frac{\alpha}{1+x(n)^2}, \tag{4.3}$$

$$y(n) = \mu(x(n) - \sigma). \tag{4.4}$$

Putting two equations together:

$$-\frac{\alpha}{1+x(n)^2} = \mu(x(n) - \sigma), \tag{4.5}$$

i.e.

$$\mu(x(n) - \sigma)\left(1 + x(n)^2\right) + \alpha = 0, \tag{4.6}$$

i.e.

$$x(n)^3 - \sigma x(n)^2 + x(n) - \sigma + \frac{\alpha}{\mu} = 0. \tag{4.7}$$

According to the method of solving the equation of degree 3 [64], by solving Eq. 4.7, we obtain $a = -\sigma$, $b = 1$, $c = -\sigma + \frac{\alpha}{\mu}$, so $p = 1 - \frac{\sigma^2}{3}$, and $q = \frac{\alpha}{\mu} - \frac{2\sigma}{3} - \frac{2\sigma^3}{27}$. The eigenvalues of Eq. 4.7 are equal to $\Delta = \frac{\left(\frac{2\sigma^3}{27}+\frac{2\sigma}{3}-\frac{\alpha}{\mu}\right)^2}{4} - \frac{\left(\frac{\sigma^2}{3}-1\right)^3}{27}$, so the equilibrium points of the model in terms of Δ states are equal to:

- If $\Delta > 0$,

$$x = \frac{\sigma}{3} + \left(\frac{\sigma}{3} - \frac{\alpha}{2\mu} + \sqrt{\frac{\left(\frac{2\sigma^3}{27}+\frac{2\sigma}{3}-\frac{\alpha}{\mu}\right)^2}{4} - \frac{\left(\frac{\sigma^2}{3}-1\right)^3}{27}} + \frac{\sigma^3}{27}\right)^{\frac{1}{3}} + \left(\frac{\sigma}{3} - \frac{\alpha}{2\mu} - \sqrt{\frac{\left(\frac{2\sigma^3}{27}+\frac{2\sigma}{3}-\frac{\alpha}{\mu}\right)^2}{4} - \frac{\left(\frac{\sigma^2}{3}-1\right)^3}{27}} + \frac{\sigma^3}{27}\right)^{\frac{1}{3}}, \tag{4.8}$$

i.e.

$$y = \mu\left(\left(\frac{\sigma}{3} - \frac{\alpha}{2\mu} + \sqrt{\frac{\left(\frac{2\sigma^3}{27}+\frac{2\sigma}{3}-\frac{\alpha}{\mu}\right)^2}{4} - \frac{\left(\frac{\sigma^2}{3}-1\right)^3}{27}} + \frac{\sigma^3}{27}\right)^{\frac{1}{3}} - \frac{2\sigma}{3} + \left(\frac{\sigma}{3} - \frac{\alpha}{2\mu} - \sqrt{\frac{\left(\frac{2\sigma^3}{27}+\frac{2\sigma}{3}-\frac{\alpha}{\mu}\right)^2}{4} - \frac{\left(\frac{\sigma^2}{3}-1\right)^3}{27}} + \frac{\sigma^3}{27}\right)^{\frac{1}{3}}\right), \tag{4.9}$$

- If $\Delta = 0$,

$$x_1 = \frac{\sigma}{3} - 2\left(\frac{\alpha}{2\mu} - \frac{\sigma}{3} - \frac{\sigma^3}{27}\right)^{\frac{1}{3}}, \tag{4.10}$$

$$x_2 = x_3 = \frac{\sigma}{3} + \left(\frac{\alpha}{2\mu} - \frac{\sigma}{3} - \frac{\sigma^3}{27}\right)^{\frac{1}{3}}, \tag{4.11}$$

i.e.

$$y_1 = -\mu\left(\frac{2\sigma}{3} + \left(\frac{\alpha}{2\mu} - \frac{\sigma}{3} - \frac{\sigma^3}{27}\right)^{\frac{1}{3}}\right), \tag{4.12}$$

$$y_2 = x_3 = -\mu\left(\frac{2\sigma}{3} - \left(\frac{\alpha}{2\mu} - \frac{\sigma}{3} - \frac{\sigma^3}{27}\right)^{\frac{1}{3}}\right), \tag{4.13}$$

- If $\Delta < 0$,

$$x_1 = \frac{\sigma}{3} - \frac{2\sqrt{3}sinsin\left(\frac{\left(\frac{3\sqrt{3}\left(\frac{2\sigma^3}{27}+\frac{2\sigma}{3}-\frac{\alpha}{\mu}\right)}{2\left(\frac{\sigma^2}{3}-1\right)^{\frac{3}{2}}}\right)}{3}\right)\sqrt{\left(\frac{\sigma^2}{3}-1\right)}}{3}, \tag{4.14}$$

$$x_2 = \frac{\sigma}{3} - \frac{2\sqrt{3}sinsin\left(\frac{\pi}{3}-\frac{\left(\frac{3\sqrt{3}\left(\frac{2\sigma^3}{27}+\frac{2\sigma}{3}-\frac{\alpha}{\mu}\right)}{2\left(\frac{\sigma^2}{3}-1\right)^{\frac{3}{2}}}\right)}{3}\right)\sqrt{\left(\frac{\sigma^2}{3}-1\right)}}{3}, \tag{4.15}$$

$$x_3 = \frac{\sigma}{3} - \frac{2\sqrt{3}sinsin\left(\frac{\pi}{6}-\frac{\left(\frac{3\sqrt{3}\left(\frac{2\sigma^3}{27}+\frac{2\sigma}{3}-\frac{\alpha}{\mu}\right)}{2\left(\frac{\sigma^2}{3}-1\right)^{\frac{3}{2}}}\right)}{3}\right)\sqrt{\left(\frac{\sigma^2}{3}-1\right)}}{3}, \tag{4.16}$$

i.e.

$$y_1 = -\mu\left(\frac{2\sigma}{3} + \frac{2\sqrt{3}sinsin\left(\frac{\left(\frac{3\sqrt{3}\left(\frac{2\sigma^3}{27}+\frac{2\sigma}{3}-\frac{\alpha}{\mu}\right)}{2\left(\frac{\sigma^2}{3}-1\right)^{\frac{3}{2}}}\right)}{3}\right)\sqrt{\left(\frac{\sigma^2}{3}-1\right)}}{3}\right), \tag{4.17}$$

$$y_2 = -\mu\left(\frac{2\sigma}{3} + \frac{2\sqrt{3}sinsin\left(\frac{\pi}{3} - \frac{\left(\frac{3\sqrt{3}\left(\frac{2\sigma^3}{27} + \frac{2\sigma}{3} - \frac{\alpha}{\mu}\right)}{2\left(\frac{\sigma^2}{3} - 1\right)^{\frac{3}{2}}}\right)}{3}\right)\sqrt{\left(\frac{\sigma^2}{3} - 1\right)}}{3}\right), \tag{4.18}$$

$$y_3 = -\mu\left(\frac{2\sigma}{3} + \frac{2\sqrt{3}sinsin\left(\frac{\pi}{6} - \frac{\left(\frac{3\sqrt{3}\left(\frac{2\sigma^3}{27} + \frac{2\sigma}{3} - \frac{\alpha}{\mu}\right)}{2\left(\frac{\sigma^2}{3} - 1\right)^{\frac{3}{2}}}\right)}{3}\right)\sqrt{\left(\frac{\sigma^2}{3} - 1\right)}}{3}\right). \tag{4.19}$$

Thus, the equilibrium points of the system are calculated, and we use the following theorem to examine the stability conditions of the equilibrium points of the fractional order system.

Theorem 2. *The zero equilibrium point of the system:*

$$\Delta_a^q F(t) = MF(t + q - 1), \tag{4.20}$$

is asymptotically stable when the eigenvalues $\lambda_i, i = 1, 2, \ldots, n$ *of the matrix* M *have the following two conditions* [65]:

$$|Arg(\lambda_i)| > \frac{q\pi}{2}, \tag{4.21}$$

$$|\lambda_i| < \left(2\,cos\,cos\left[\frac{|Arg(\lambda_i)| - \pi}{2 - q}\right]\right)^q. \tag{4.22}$$

Therefore, we calculate the Jacobian matrix of Eq. 3.1, and Eq. 3.2, which is as follows:

$$J = \left[\frac{2\alpha x(n)}{(x(n)^2+1)^2}\ 1\ -\mu\ 1\right]. \tag{4.23}$$

The eigenvalues of the Jacobin matrix are calculated for equilibrium points at different parameters, and the conditions of Theorem 2 are obtained numerically for the eigenvalues. The parameters that

satisfy the Theorem 2 requirements make Eq. 3.1, and Eq. 3.2 always stable.

4.1. Stability regions of the FORNM

The stability regions of the equilibrium points of the FORNM model have been investigated by varying the parameters in the model. The fractional order in the FORNM model is examined in the first step. Stability regions of the FORNM model are shown in Figure 6 in the three-dimensional space of $\alpha - \sigma - \mu$ parameters and the two-dimensional space of parameters $\alpha - \sigma$, $\alpha - \mu$, and $\sigma - \mu$. The fractional order in parts (a-c) are $q = 0.001$, $q = 0.01$, $q = 0.025$ respectively. It is shown that the stable regions decrease by increasing the value of fractional order.

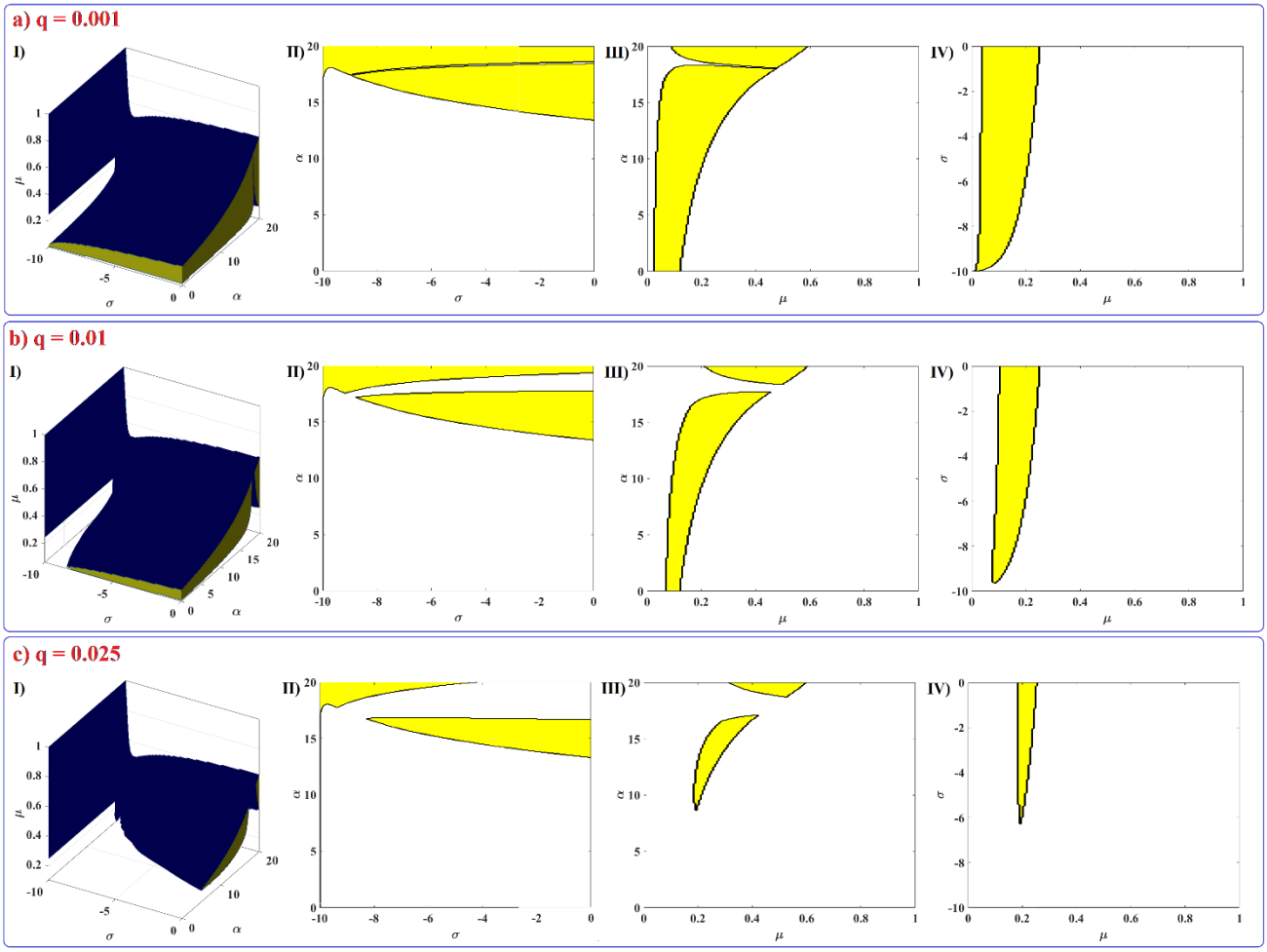

Figure 6. The stability regions of the FORNM model with **(a)** $q = 0.001$, **(b)** $q = 0.01$, and **(c)** $q = 0.025$. **(I)** In the $\alpha - \sigma - \mu$ parameter space, **(II)** in the $\alpha - \sigma$ parameter space, **(III)** in the $\alpha - \mu$ parameter space, and **(IV)** in the $\sigma - \mu$ parameter space.

In the second step, the effects of $q - \sigma - \mu$ parameters with $\alpha = 15$ constant in part (a), the effects of $\alpha - q - \mu$ parameters with $\sigma = -5$ constant in part (b), and the effects of $\alpha - \sigma - q$ parameters with constant $\mu = 0.3$ in part (c) on the stability of the FORNM model are investigated and shown in Figure 7. In part (a) of Figure 7, the stability of the system is lost as the value of σ increases toward zero, and the stability of the system is lost as μ increases toward one. In part (b) of Figure 7, the stability of the

system increases with the increase of α value, and the stability of the system decreases with the increase of μ. In part (c) of Figure 7, by increasing the value of α and σ, stability is created in the system.

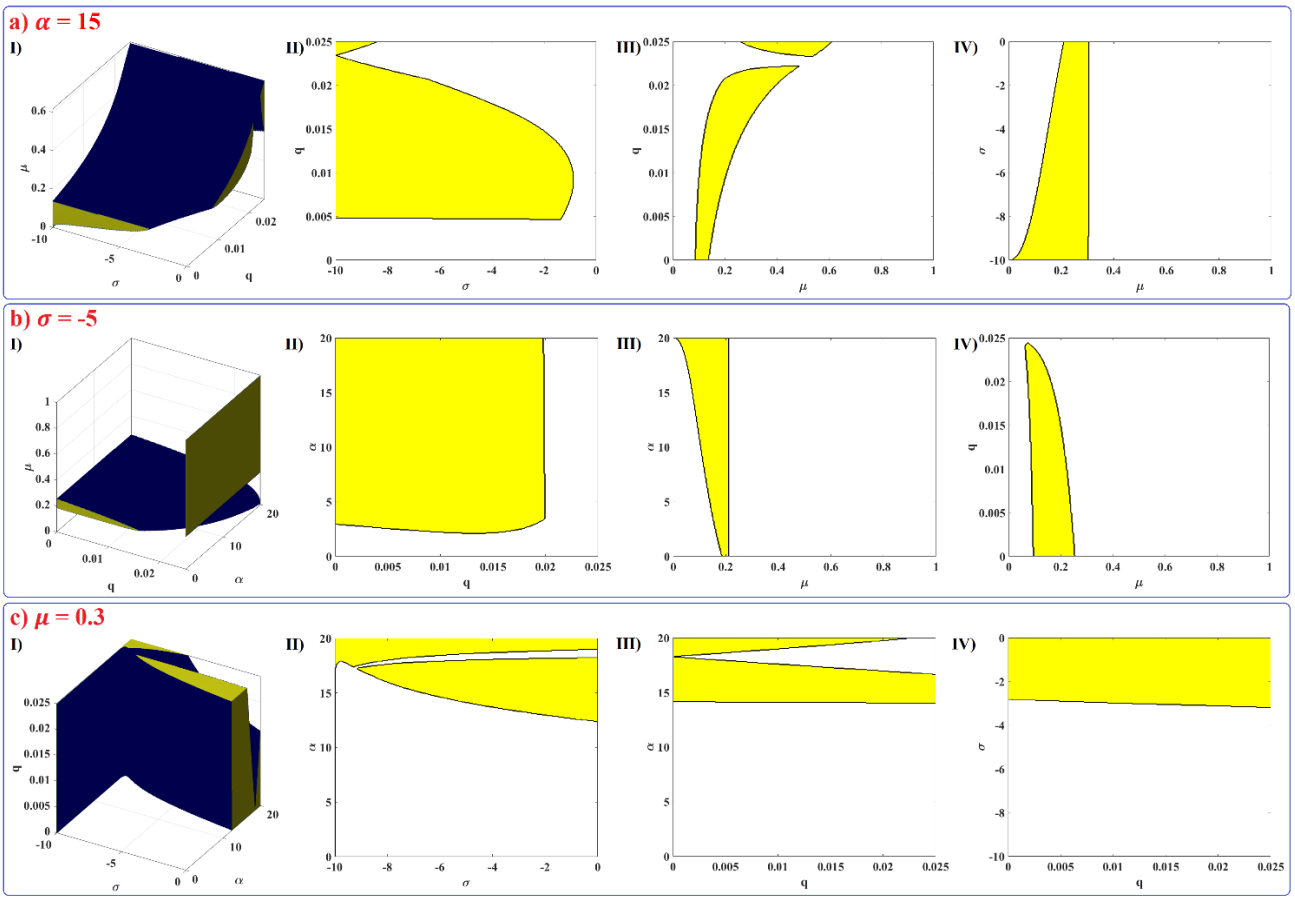

Figure 7. The stability regions of the FORNM model with **(a)** $\alpha = 15$, **(b)** $\sigma = -5$, and **(c)** $\mu = 0.3$ in 2D and 3D parameter planes.

5. Synchronization of FORNM

Another important aspect of the dynamical analysis is the synchronization in a chaotic state. Two coupled fractional-order Rulkov neuron maps can be formulated as follows:

$$x_1(n) = x_1(0) + \frac{1}{\Gamma(q)}\sum_{i=1}^{n} \frac{\Gamma(n-i+q)}{\Gamma(n-i+1)}\left(\frac{\alpha}{1+x_1(i-1)^2} + y_1(i-1)\right) + d_x\big(x_2(n) - x_1(n)\big), \quad (4.24)$$

$$y_1(n) = y_1(0) + \frac{1}{\Gamma(q)}\sum_{i=1}^{n} \frac{\Gamma(n-i+q)}{\Gamma(n-i+1)}\big(y_1(i-1) - \mu(x_1(i-1) - \sigma)\big) + d_y\big(y_2(n) - y_1(n)\big), \quad (4.25)$$

$$x_2(n) = x_2(0) + \frac{1}{\Gamma(q)}\sum_{i=1}^{n} \frac{\Gamma(n-i+q)}{\Gamma(n-i+1)}\left(\frac{\alpha}{1+x_2(i-1)^2} + y_2(i-1)\right) + d_x\big(x_1(n) - x_2(n)\big), \quad (4.26)$$

$$y_2(n) = y_2(0) + \frac{1}{\Gamma(q)}\sum_{i=1}^{n} \frac{\Gamma(n-i+q)}{\Gamma(n-i+1)}\big(y_2(i-1) - \mu(x_2(i-1)-\sigma)\big) + d_y\big(y_1(n) - y_2(n)\big), \quad (4.27)$$

where subscript 1 corresponds to neuron one and subscript two corresponds to neuron 2, d_x is the coupling strength of variable $x(n)$, and d_y is the coupling strength of variable $y(n)$. For both neuron models, the initial conditions are randomly chosen between -1 and 1. To determine the synchronization level of two neurons, the average error is calculated in the form of the following equation:

$$Error = \sqrt{\frac{1}{N}\sum_{j=1}^{N} \big(x_1(n) - x_2(n)\big)^2 + \big(y_1(n) - y_2(n)\big)^2}, \quad (4.28)$$

where N represents the number of time series data samples. We investigate the effects of fractional order changes on the synchronization of neurons. Figure 8 shows the synchronization error by changing the coupling strengths d_x and d_y in different fractional orders. It has been proven that two integer-order Rulkov maps cannot reach synchronization when connected by electrical synapses [66]. Here, it can be seen that the synchronization cannot occur in the fractional-order neurons too. It should be noted that the systems become unstable for coupling coefficients higher than 1. Unsynchronized neuron maps based on previous papers show that increased activity in certain areas is accompanied by decreased activity in other areas [67], and this pattern exists during rest and sleep [68].

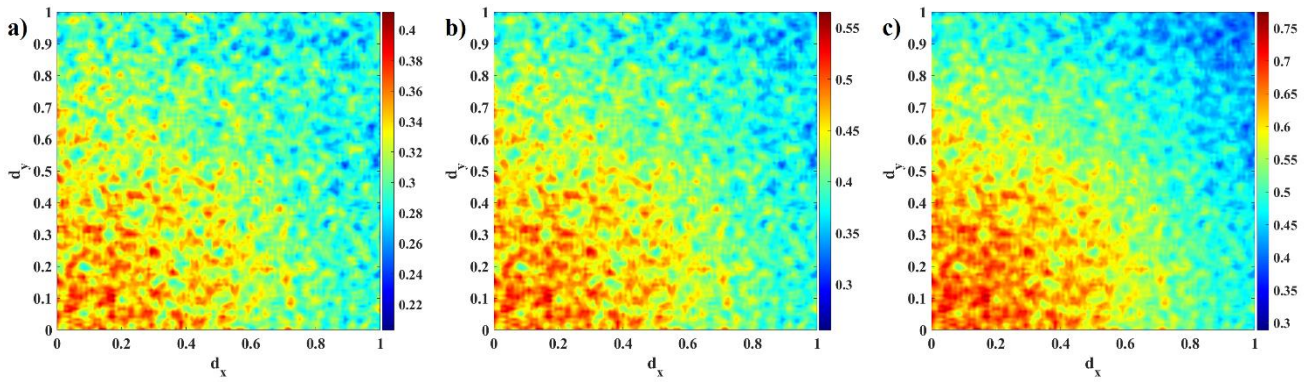

Figure 8. The synchronization error of two coupled fractional Rulkov neurons in terms of d_x and d_y for **(a)** $q = 0.001$, **(b)** $q = 0.005$, and **(c)** $q = 0.01$. The parameters of the model are $\alpha = 6$, $\sigma = -1$, and $\mu = 0.3$.

6. Conclusion

This paper proposed the discrete fractional order Rulkov neuron map in Caputo's concept. The dynamic analysis of the fractional model was performed, and its synchronization was evaluated. Adding discrete fraction calculus to the Rulkov neuron map can consider the effect of memory on neural model dynamics. Memory effects refer to the fact that system states are determined in fractional order by all previous states. At first, the Rulkov neuron map was examined in terms of phase plane, bifurcation diagram, and Lyapunov exponent. It was shown that the biological behaviors of the Rulkov neuron map, such as silence, bursting, and chaotic firing, also exist in the discrete fractional order Rulkov neuron map. Hence, the Rulkov neuron map of discrete fractional order shows the same behaviors as the Rulkov map of integer order. However, changing the fractional order can result in

bifurcation. In the next step, the stability regions of the system from a theoretical and numerical point of view were examined and it was shown that increasing the order of the fraction decreases the stability in the FORNM system. In the last stage, the synchronization behavior of two FORNM systems was investigated. The results showed that the fractional-order systems do not achieve synchronization with an increase in the coupling coefficient, which is similar to the integer-order systems. Table 1 shows the reason for the superiority of the result of Rulkov fractional neuron map to the previous works.

Table 1. Comparison of the proposed model with previous works.

Ref	Year	Model	Description
[69]	2021	Nagumo–Sato discrete neuron map	A fractional-order version of the one-dimensional neuron map is proposed. The dynamic behavior of the model has been analyzed by drawing bifurcation diagrams and the Lyapunov power diagram. The appearance of the spiral wave in the two-dimensional network for the fractional order version has been investigated in terms of the effect of various parameters such as the amplitude and frequency of stimuli, the coupling strength, and the fractional order parameter.
[70]	2021	Rulkov Neuron Map	A theoretical investigation is done on a fractional order version of the Rulkov neural model, which is only the time series analysis of the proposed model, and its dynamic behavior is not evaluated.
[71]	2022	Rulkov Neuron Map	In this research, the model has been implemented by applying discrete memristor on two-dimensional Rulkov neuron map. The dynamic behaviors of the discrete memristor-based neuron have been analyzed by experiments including phase diagram, bifurcation, and spectral entropy complexity algorithm. In this system, the intended memory, which is the inheritance of information transmission, is not considered.
[72]	2020	Rulkov Neuron Map	A theoretical investigation for the asymptotic stability and instability of two-dimensional independent linearly incommensurate systems of fractional order Caputo difference equations has been carried out. In this article, only the time series analysis of the proposed model is done and its dynamic behavior is not evaluated.
-	-	Proposed Model	In this research, the fractional order discrete Rulkov neuron map is analyzed in terms of dynamic behavior and synchronization. Biological behaviors of the Rulkov neuron map, such as silence, bursting, and chaotic firing, are also present in its discrete fractional order version. The bifurcation diagrams of the proposed model are investigated under the influence of neuronal model parameters and fractional order. The stability regions of the system are obtained theoretically and numerically, and it is shown that increasing the order of the fractional order causes the reduction of the stable regions. In general, the hereditary behavior of the neural model is proposed using discrete fractional order.

For future work, discrete fractional order derivatives can be implemented on DNA-based genetic systems to investigate hereditary factors, so that human evolution can be described from these systems. For the next research topic, different types of discrete fractional order derivatives can be evaluated on the Rulkov neuron map. Due to the fact that the Rulkov discrete neuron map has no synchronization power, different controllers can be used to check synchronization.

Acknowledgments

This work is partially funded by Centre for Nonlinear Systems, Chennai Institute of Technology, India, vide funding number CIT/CNS/2023/RP/005.

Conflict of interest

The authors declare that they have no conflict of interest.

References

1. F. Corinto, A. Torcini, *Nonlinear dynamics in computational neuroscience*, Springer, 2019. https://doi.org/10.1007/978-3-319-71048-8
2. D. Sterratt, B. Graham, A. Gillies, D. Willshaw, *Principles of computational modelling in neuroscience*, Cambridge University Press, 2011.
3. J. F. Tagne, H. C. Edima, Z. T. Njitacke, F. F. Kemwoue, R. N. Mballa, J. Atangana, Bifurcations analysis and experimental study of the dynamics of a thermosensitive neuron conducted simultaneously by photocurrent and thermistance, *Eur. Phys. J. Spec. Top*, **231** (2022), 993–1004. https://doi.org/10.1140/epjs/s11734-021-00311-w
4. E. M. Izhikevich, *Dynamical systems in neuroscience*, MIT press, 2007.
5. D. Guo, S. Wu, M. Chen, M. Perc, Y. Zhang, J. Ma, et al., Regulation of irregular neuronal firing by autaptic transmission, *Sci. Rep.*, **6** (2016), 1–14. https://doi.org/10.1038/srep26096
6. J. Ma, J. Tang, A review for dynamics in neuron and neuronal network, *Nonlinear Dyn.*, **89** (2017), 1569–1578. https://doi.org/10.1007/s11071-017-3565-3
7. A. Foroutannia, M. Ghasemi, F. Parastesh, S. Jafari, M. Perc, Complete dynamical analysis of a neocortical network model, *Nonlinear Dyn.*, **100** (2020), 2699–2714. https://doi.org/10.1007/s11071-020-05668-6
8. Q. Xu, X. Tan, D. Zhu, H. Bao, Y. Hu, B. Bao, Bifurcations to bursting and spiking in the Chay neuron and their validation in a digital circuit, *Chaos Solit. Fract.*, **141** (2020), 110353. https://doi.org/10.1016/j.chaos.2020.110353
9. A. L. Hodgkin, A. F. Huxley, A quantitative description of membrane current and its application to conduction and excitation in nerve, *J. Physiol.*, **117** (1952), 500. https://doi.org/10.1113%2Fjphysiol.1952.sp004764
10. R. FitzHugh, Impulses and physiological states in theoretical models of nerve membrane, *Biophys. J.*, **1** (1961), 445–466. https://doi.org/10.1016/S0006-3495(61)86902-6
11. Z. T. Njitacke, C. N. Takembo, J. Awrejcewicz, H. P. E. Fouda, J. Kengne, Hamilton energy, complex dynamical analysis and information patterns of a new memristive FitzHugh-Nagumo neural network, *Chaos Solit. Fract.*, **160** (2022), 112211. https://doi.org/10.1016/j.chaos.2022.112211
12. J. L. Hindmarsh, R. Rose, A model of neuronal bursting using three coupled first order differential equations, *Proc. R Soc. London Ser. B*, **221** (1984), 87–102. https://doi.org/10.1098/rspb.1984.0024
13. Z. T. Njitacke, J. Awrejcewicz, A. N. K. Telem, T. F. Fozin, J. Kengne, Complex dynamics of coupled neurons through a memristive synapse: extreme multistability and its control with selection of the desired state, *IEEE Trans. Circuits Syst. II Express Briefs*, (2022). https://doi.org/10.1109/TCSII.2022.3172141
14. Z. T. Njitacke, T. F. Fozin, S. S. Muni, J. Awrejcewicz, J. Kengne, Energy computation, infinitely coexisting patterns and their control from a Hindmarsh–Rose neuron with memristive autapse: Circuit implementation, *AEU Int. J. Electron. Commun.*, **155** (2022), 154361. https://doi.org/10.1016/j.aeue.2022.154361
15. Z. N. Tabekoueng, S. S. Muni, T. F. Fozin, G. D. Leutcho, J. Awrejcewicz, Coexistence of infinitely many patterns and their control in heterogeneous coupled neurons through a multistable memristive synapse, *Chaos*, **32** (2022), 053114. https://doi.org/10.1063/5.0086182

16. B. Ibarz, J. M. Casado, M. A. Sanjuán, Map-based models in neuronal dynamics, *Phys. Rep.*, **501** (2011), 1–74. https://doi.org/10.1016/j.physrep.2010.12.003
17. M. Gosak, M. Milojević, M. Duh, K. Skok, M. Perc, Networks behind the morphology and structural design of living systems, *Phys. Life Rev.* (2022). https://doi.org/10.1016/j.plrev.2022.03.001
18. S. Majhi, M. Perc, D. Ghosh, Dynamics on higher-order networks: A review, *J. R Soc. Interf.*, **19** (2022), 20220043. https://doi.org/10.1098/rsif.2022.0043
19. M. Perc, Spatial coherence resonance in neuronal media with discrete local dynamics, *Chaos Solit. Fract.*, **31** (2007), 64–69. https://doi.org/10.1016/j.chaos.2005.09.021
20. E. M. Izhikevich, Simple model of spiking neurons, *IEEE Trans. Neural Networks*, **14** (2003), 1569–1572. https://doi.org/10.1109/TNN.2003.820440
21. J. Nagumo, S. Sato, On a response characteristic of a mathematical neuron model, *Kybernetik*, **10** (1972), 155–164. https://doi.org/10.1007/BF00290514
22. K. Aihara, T. Takabe, M. Toyoda, Chaotic neural networks, *Phys. Lett. A*, **144** (1990), 333–340. https://doi.org/10.1016/0375-9601(90)90136-C
23. F. Pasemann, A simple chaotic neuron, *Physica D*, **104** (1997), 205–211. https://doi.org/10.1016/S0167-2789(96)00239-4
24. N. F. Rulkov, Modeling of spiking-bursting neural behavior using two-dimensional map, *Phys. Rev. E*, **65** (2002), 041922. https://doi.org/10.1103/PhysRevE.65.041922
25. N. F. Rulkov, Regularization of synchronized chaotic bursts, *Phys. Rev. Lett.*., **86** (2001), 183. https://doi.org/10.1103/PhysRevLett.86.183
26. M. Mehrabbeik, F. Parastesh, J. Ramadoss, K. Rajagopal, H. Namazi, S. Jafari, Synchronization and chimera states in the network of electrochemically coupled memristive Rulkov neuron maps, *Math. Biosci. Eng.*, **18** (2021), 9394–9409. https://doi.org/10.3934/mbe.2021462
27. B. Bao, J. Hu, J. Cai, X. Zhang, H. Bao, Memristor-induced mode transitions and extreme multistability in a map-based neuron model, *Nonlinear Dyn.*. (2022), 1–15. https://doi.org/10.1007/s11071-022-07981-8
28. K. Li, B. Bao, J. Ma, M. Chen, H. Bao, Synchronization transitions in a discrete memristor-coupled bi-neuron model, *Chaos Solit. Fract.*, **165** (2022), 112861. https://doi.org/10.1016/j.chaos.2022.112861
29. H. Sun, H. Cao, Synchronization of two identical and non-identical Rulkov models, *Commun. Nonlinear Sci. Numer. Simul.*, **40** (2016), 15–27. https://doi.org/10.1016/j.cnsns.2016.04.011
30. I. Franović, V. Miljković, The effects of synaptic time delay on motifs of chemically coupled Rulkov model neurons, *Commun. Nonlinear Sci. Numer. Simul.*, **16** (2011), 623–633. https://doi.org/10.1016/j.cnsns.2010.05.007
31. S. Rakshit, A. Ray, B. K. Bera, D. Ghosh, Synchronization and firing patterns of coupled Rulkov neuronal map, *Nonlinear Dyn.*, **94** (2018), 785–805. https://doi.org/10.1007/s11071-018-4394-8
32. A. Wagemakers, M. A. Sanjuán, Electronic circuit implementation of the chaotic Rulkov neuron model, *J. Franklin Inst.*, **350** (2013), 2901–2910. https://doi.org/10.1016/j.jfranklin.2013.01.026
33. K. Li, H. Bao, H. Li, J. Ma, Z. Hua, B. Bao, Memristive Rulkov neuron model with magnetic induction effects, *IEEE Trans. Ind. Inf.*, **18** (2021), 1726–1736. https://doi.org/10.1109/TII.2021.3086819
34. L. Cheng, H. Cao, Synchronization dynamics of two heterogeneous chaotic Rulkov neurons with electrical synapses, *Int. J. Bifurc. Chaos*, **27** (2017), 1730009.

https://doi.org/10.1142/S0218127417300099
35. J. Ma, Biophysical neurons, energy, and synapse controllability: A review, *J. Zhejiang Univ. Sci. A*, (2022).
36. Y. Xie, Z. Yao, J. Ma, Phase synchronization and energy balance between neurons, *Front. Inf. Technol. Electron. Eng.*, (2022), 1–14. https://doi.org/10.1631/FITEE.2100563
37. M. Rahimy, Applications of fractional differential equations, *Appl. Math. Sci.*, **4** (2010), 2453–2461.
38. L.-L. Huang, G.-C. Wu, D. Baleanu, H.-Y. Wang, Discrete fractional calculus for interval–valued systems, *Fuzzy Sets Syst.*, **404** (2021), 141–158. https://doi.org/10.1016/j.fss.2020.04.008
39. F. M. Atici, P. Eloe, Discrete fractional calculus with the nabla operator, *Electron. J. Qual. Theory Differ Equ.*, **2009** (2009), 12, electronic only. https://doi.org/10.14232/ejqtde.2009.4.3
40. G. A. Anastassiou, Principles of delta fractional calculus on time scales and inequalities, *Math. Comput. Modell.*, **52** (2010), 556–566. https://doi.org/10.1016/j.mcm.2010.03.055
41. Y. Wang, K. Sun, S. He, H. Wang, Dynamics of fractional-order sinusoidally forced simplified Lorenz system and its synchronization, *Eur. Phys. J. Spec. Top*, **223** (2014), 1591–1600. https://doi.org/10.1140/epjst/e2014-02181-3
42. K. Rajagopal, A. Karthikeyan, S. Jafari, F. Parastesh, C. Volos, I. Hussain, Wave propagation and spiral wave formation in a Hindmarsh–Rose neuron model with fractional-order threshold memristor synaps, *Int. J. Mod. Phys. B*, **34** (2020), 2050157. https://doi.org/10.1142/S021797922050157X
43. B. Ramakrishnan, F. Parastesh, S. Jafari, K. Rajagopal, G. Stamov, I. Stamova, Synchronization in a Multiplex Network of Nonidentical Fractional-Order Neurons, *Fractal Fract*, **6** (2022), 169. https://doi.org/10.3390/fractalfract6030169
44. W. M. Ahmad, J. C. Sprott, Chaos in fractional-order autonomous nonlinear systems, *Chaos Solit. Fract.*, **16** (2003), 339–351. https://doi.org/10.1016/S0960-0779(02)00438-1
45. L. Wang, K. Sun, Y. Peng, S. He, Chaos and complexity in a fractional-order higher-dimensional multicavity chaotic map, *Chaos Solit. Fract.*, **131** (2020), 109488. https://doi.org/10.1016/j.chaos.2019.109488
46. Y. Peng, S. He, K. Sun, Chaos in the discrete memristor-based system with fractional-order difference, *Results Phys.*, **24** (2021), 104106. https://doi.org/10.1016/j.rinp.2021.104106
47. G.-C. Wu, D. Baleanu, Discrete chaos in fractional delayed logistic maps, *Nonlinear Dyn.*, **80** (2015), 1697–1703. https://doi.org/10.1007/s11071-014-1250-3
48. A. Elsonbaty, Z. Sabir, R. Ramaswamy, W. Adel, Dynamical analysis of a novel discrete fractional SITRs model for COVID-19, *Fractals*, (2021), 2140035. https://doi.org/10.1142/S0218348X21400351
49. S. Kassim, H. Hamiche, S. Djennoune, M. Bettayeb, A novel secure image transmission scheme based on synchronization of fractional-order discrete-time hyperchaotic systems, *Nonlinear Dyn.*, **88** (2017), 2473–2489. https://doi.org/10.1007/s11071-017-3390-8
50. M. R. Dar, N. A. Kant, F. A. Khanday, Dynamics and implementation techniques of fractional-order neuron models: A survey, *Fract. Order Syst.*, (2022), 483–511. https://doi.org/10.1016/B978-0-12-824293-3.00017-X
51. D. M. Gash, A. S. Deane, Neuron-based heredity and human evolution, *Front. Neurosci.*, **9** (2015), 209. https://doi.org/10.3389%2Ffnins.2015.00209
52. S. Rakshit, S. Majhi, J. Kurths, D. Ghosh, Neuronal synchronization in long-range time-varying

networks, *Chaos*, **31** (2021), 073129. https://doi.org/10.1063/5.0057276
53. Q. Xu, T. Liu, S. Ding, H. Bao, Z. Li, B. Chen, Extreme multistability and phase synchronization in a heterogeneous bi-neuron Rulkov network with memristive electromagnetic induction, *J. Cogn. Neurosci.,*, (2022), 1–12. https://doi.org/10.1007/s11571-022-09866-3
54. K. Clark, R. F. Squire, Y. Merrikhi, B. Noudoost, Visual attention: Linking prefrontal sources to neuronal and behavioral correlates, *Prog. Neurobiol.*, **132** (2015), 59–80. https://doi.org/10.1016/j.pneurobio.2015.06.006
55. J. Ma, J. Tang, A review for dynamics of collective behaviors of network of neurons, *Sci. China Technol. Sci.*, **58** (2015), 2038–2045. https://doi.org/10.1007/s11431-015-5961-6
56. J. Munkhammar, Chaos in a fractional order logistic map, *Fract. Calc. Appl. Anal.*, **16** (2013), 511–519. https://doi.org/10.2478/s13540-013-0033-8
57. M.-F. Danca, Puu system of fractional order and its chaos suppression, *Symmetry*, **12** (2020), 340. https://doi.org/10.3390/sym12030340
58. T. Abdeljawad, On Riemann and Caputo fractional differences, *Comput. Math. Appl.*, **62** (2011), 1602–1611. https://doi.org/10.1016/j.camwa.2011.03.036
59. M. T. Holm, The Laplace transform in discrete fractional calculus, *Comput. Math. Appl.*, **62** (2011), 1591–1601. https://doi.org/10.1016/j.camwa.2011.04.019
60. F. Atici, P. Eloe, Initial value problems in discrete fractional calculus, *Proc. Am. Math. Soc.*, **137** (2009), 981–989. https://doi.org/10.1090/S0002-9939-08-09626-3
61. A. Chen, Y. Chen, Existence of solutions to anti-periodic boundary value problem for nonlinear fractional differential equations with impulses, *Adv. Differ. Equat.*, **2011** (2011), 1–17. https://doi.org/10.1155/2011/915689
62. W. Gerstner, W. M. Kistler, *Spiking neuron models: Single neurons, populations, plasticity*, Cambridge university press, 2002.
63. A. Gangopadhyay, D. Mehta, S. Chakrabartty, A spiking neuron and population model based on the growth transform dynamical system, *Front. Neurosci.*, **14** (2020), 425. https://doi.org/10.3389/fnins.2020.00425
64. R. Nickalls, Viete, Descartes and the cubic equation, *Math. Gaz.*, **90** (2006), 203–208. https://doi.org/10.1017/S0025557200179598
65. J. Čermák, I. Győri, L. Nechvátal, On explicit stability conditions for a linear fractional difference system, *Fract. Calc. Appl. Anal.*, **18** (2015), 651–672. https://doi.org/10.1515/fca-2015-0040
66. H. Sun, H. Cao, Complete synchronization of coupled Rulkov neuron networks, *Nonlinear Dyn.*, **84** (2016), 2423–2434. https://doi.org/10.1007/s11071-016-2654-z
67. D. A. Gusnard, M. E. Raichle, Searching for a baseline: Functional imaging and the resting human brain, *Nat. Rev. Neurosci.*, **2** (2001), 685–694. https://doi.org/10.1038/35094500
68. S. G. Horovitz, A. R. Braun, W. S. Carr, D. Picchioni, T. J. Balkin, M. Fukunaga, et al., Decoupling of the brain's default mode network during deep sleep, *Proc. Natl. Acad. Sci.*, **106** (2009), 11376–11381. https://doi.org/10.1073/pnas.0901435106
69. K. Rajagopal, S. Panahi, M. Chen, S. Jafari, B. Bao, Suppressing spiral wave turbulence in a simple fractional-order discrete neuron map using impulse triggering, *Fractals*, **29** (2021), 2140030. https://doi.org/10.1142/S0218348X21400302
70. O. Brandibur, E. Kaslik, D. Mozyrska, M. Wyrwas, A Rulkov neuronal model with Caputo fractional variable-order differences of convolution type, *Dynam. Syst. Theory Appl.*, (2019), 227–235. https://doi.org/10.1007/978-3-030-77310-6_20

71. L. J. Liu, Y. H. Qin, Dynamics of discrete memristor-based Rulkov neuron, *IEEE Access*, **10** (2022), 72051–72056. https://doi.org/10.1109/ACCESS.2022.3188787
72. O. Brandibur, E. Kaslik, D. Mozyrska, M. Wyrwas, Stability of systems of fractional-order difference equations and applications to a Rulkov-type neuronal model, *New Trends Nonlinear Dyn.*, (2020), 305–314. https://doi.org/10.1007/978-3-030-34724-6_31

AIMS Press